Journal of Power Sources 258 (2014) 266–271

Contents lists available at ScienceDirect

Journal of Power Sources

journal homepage: www.elsevier.com/locate/jpowsour

Structural evolution and electrochemistry of monoclinic $NaNiO_2$ upon the first cycling process

Man Huon Han [a,*], Elena Gonzalo [a,1], Montse Casas-Cabanas [a,1], Teófilo Rojo [a,b,1,2]

[a] CICenergigune, Parque Tecnológico de Álava, Albert Einstein 48, ED.CIC, 01510 Miñano, Spain
[b] Departamento de Química Inorgánica, Universidad del País Vasco UPV/EHU, P.O. Box 644, 48080 Bilbao, Spain

HIGHLIGHTS

- Structural evolution of $NaNiO_2$ is studied by means of *in situ* XRD.
- Each phase transition and Na contents are characterized.
- The capacity retention for first 25 cycles is investigated.

ARTICLE INFO

Article history:
Received 2 December 2013
Received in revised form
22 January 2014
Accepted 11 February 2014
Available online 21 February 2014

Keywords:
$NaNiO_2$
Intercalation/deintercalation mechanism
In situ XRD techniques
Na-ion cathode

ABSTRACT

Electrochemistry and structural evolution of monoclinic $NaNiO_2$ as a cathode material for Na-ion battery is reported. The initial charge capacity reached 160 mA h g^{-1} and the following discharge capacity of 114.6 mA h g^{-1}, within the voltage range of 4.0–1.5 V at C/10. The multiple phase transition leading to O′3, P′3, P″3, O″3, and O‴3 stacking types ($NaNiO_2$, $Na_{0.91}NiO_2$, $Na_{0.84}NiO_2$, $Na_{0.81}NiO_2$ and $Na_{0.79}NiO_2$ transitions, respectively, according to a previous report) during the 1st charge/discharge process is analysed using *ex situ* and *in situ* XRD techniques, and the stoichiometry of each phase is herein revised. The charge/discharge profile shows a highly reversible nature of the cathode, except that fully sodiated phase could not be achieved at the subsequent discharge. Two new phases have been discovered: a monoclinic O3 structure (designated as O⁗3) at the beginning of the charge (and end of discharge) and a P3 structure (designated as P‴3) at 3.38 V that appeared only during the charge process. The composition of the new O⁗3-phase corresponds to $Na_{0.83}NiO_2$, which is the closest to the fully sodiated phase at room temperature achieved during the discharge process reported up to date, and the composition of the new P‴3-phase corresponds approximately to $Na_{0.50}NiO_2$.

1. Introduction

Recently, Na-ion batteries have received substantial attention for their advantages over Li-ion batteries, such as the availability of sodium over wide geographic sites. It is widely believed that Na-ion cathode materials cannot match the energy density of Li-ion battery because sodium is more than 3 times heavier than lithium and the operation voltage is lower. However, recent investigations show a promising future for Na-ion battery as a feasible alternative in cost-driven applications, such as large scale energy storage facilities or power grid systems [1,2].

Among the possible cathode material candidates for Na-ion batteries, layered $NaMO_2$ compounds (M = V, Cr, Mn, Fe, Co, Ni, or mixture of 2–3 elements) have been studied extensively [3–5] because of their relatively simple structure and high capacity. Structurally, oxide layers consist of series of edge-sharing MO_6 octahedra in the *ab* plane while sodium ions are located in between the oxide layers [6]. The structure and electrochemical behaviour of $NaMO_2$ are similar to that of $LiMO_2$ analogues from which Li is deintercalated/intercalated from the host material to store or extract energy. However, despite their similarities, their chemistry is expected to differ because of their different ionic radii (Li^+: 0.76 Å, Na^+: 1.02 Å). For example in the case of $LiNiO_2$, it is very difficult to synthesize an ideal structure due to the similar ionic radii of Li and Ni resulting in poor electrochemical performance [7].

* Corresponding author. Tel.: +34 945297108.
E-mail addresses: mhan@cicenergigune.com (M.H. Han), egonzalo@cicenergigune.com (E. Gonzalo), mcasas@cicenergigune.com (M. Casas-Cabanas), trojo@cicenergigune.com (T. Rojo).
[1] Tel.: +34 945297108.
[2] Tel.: +34 946012458; fax: +34 946013500.

http://dx.doi.org/10.1016/j.jpowsour.2014.02.048
0378-7753/

In addition, in the case of $LiMnO_2$, a rapid capacity loss during cycling is observed due to the migration of M^{n+} into the interlayers to form the spinel structure [8]. However, such problematic phenomena have not been observed for sodium layered oxides because the ionic radius of Na^+ is significantly larger than that of M^{n+}. Therefore, formation of ideal structure is more feasible and the migration of M^{n+} into the interlayer is highly unlikely.

The first electrochemical and structural investigation of $NaNiO_2$ is dated back to 1982 by Braconnier et al. [9]. A structural analysis of the multiple phase transitions occurring up to approximately 3.7 V was shown, corresponding to the deintercalation of only 0.2 sodium ions during the first charge. A recent publication however showed that 0.85 sodium ions (199 mA h g^{-1}) could be deintercalated and 0.62 sodium ions (147 mA h g^{-1}) could be reintercalated during the first charge/discharge cycle within the voltage range of 4.5–2.0 V [10], while exhibiting the same multiple plateaus as reported in the first paper [9]. Our aim is thus to reinvestigate the phase changes in order to obtain a more detailed understanding of the structural evolution along with the electrochemical process during the deintercalation/intercalation process. In this paper, the electrochemical properties and the analysis of the successive phase changes of monoclinic O′3-phase $NaNiO_2$ at each charge/discharge plateau is studied using *ex situ* and real-time *in situ* XRD techniques. In addition, *in situ* XRD measurements after relaxation at selected charge/discharge potentials, henceforth relaxed *in situ* XRD, are also analysed using a wider 2θ range. The previously reported formation of a partially desodiated phase during electrode preparation using NMP (1-methyl-2-pyrrolidone) and PVDF (polyvinylidene fluoride) in the slurry formulation [10] is here vastly improved by implementing hydrophobic components. Similar to the most recent study [10], an initial charge capacity of 160 mA h g^{-1} and a following discharge capacity of 114.6 mA h g^{-1} are achieved within the voltage range of 4.0–1.5 V at C/10. The formation of new phases during the charge/discharge process is also reported.

2. Experimental section

Monoclinic $NaNiO_2$ was synthesized by ceramic route. Stoichiometric ratios of Na_2O_2 and NiO were hand-mixed in a glove box using a mortar and a pestle for approximately 1 h in order to obtain a homogeneous mixture of the starting reagents. The homogeneous mixture was then fired at 650 °C for 3 h under 1 bar O_2 atmosphere followed by free cooling. Upon cooling, the dark grey/black powder was transferred immediately into the glove box in order to avoid contact from atmospheric moisture. X-ray diffraction pattern of the pristine material was collected using a Bruker D8 Advanced with Cu Kα radiation of (λ = 1.5418 Å) within the 2θ range of 15–80°. All samples were mounted on an atmosphere protective XRD sample holder with Kapton film cover in order to avoid atmospheric moisture contact. Pattern matching of XRD data was performed using Fullprof software [11], and elemental analysis was carried out using Horiba Scientific Ultima 2 ICP-OES.

Electrode preparation was performed in an Ar-filled glove box. The slurry of the electrode was prepared with a mixture of active material, super carbon C65, and EPDM (ethylene propylene diene monomer rubber) as binder in the mass ratio of 80:10:10 in cyclohexane, followed by vigorous stirring for 2 h. The slurry was then hand-casted onto an aluminium current collector sheet using a Dr. Blade. The laminate was immediately transferred into the vacuum chamber and dried at room temperature under constant vacuum for 12 h before ½″ circular individual electrodes were punched out.

Ex situ XRD studies were carried out with $NaNiO_2$ laminate electrodes cycled in Na half-cells using 0.5 M $NaPF_6$ in EC (ethylene carbonate):DMC (dimethyl carbonate) electrolyte in ½″ Swagelok cells. The galvanostatic electrochemical testing was performed with a Bio-Logic VMP3 potentiostat within the voltage range of 4.0–1.5 V at C/10 rate at room temperature. All the cycled cells were disassembled in the Ar-filled glove box to collect the electrodes. The electrodes were thoroughly washed with DMC and dried under vacuum for at least 30 min before further investigation. Coin cells were also assembled for the cyclability study using the same electrolyte and cycled for 25 times within the voltage range of 4.0–2.0 V at C/10.

In situ XRD samples were prepared with a custom designed 1″ *in situ* cell equipped with Be window for XRD observation and polyoxymethylene body. A powder mixture of active material and super carbon C65 at the weight ratio of 80:20 was loaded in the cell along with 2 glass fibre separators. A proper amount of 0.5 M $NaPF_6$ in EC:DMC (1:1) electrolyte was added before closing the cell with a Na plated stainless steel plunger. The cell was galvanostatically cycled over the voltage range of 4.0–1.5 V at C/70 using a Biologic SP200 potentiostat. Each scan was collected in 0.02° increments between 15–18° and 31–38° at a scanning speed of 0.0089° s^{-1}. The relaxed *in situ* XRD experiment was performed cycling over the voltage range of 4.0–1.5 V at C/10 using Biologic VMP3 potentiostat and by stopping the cell at the desired voltage to measure the XRD

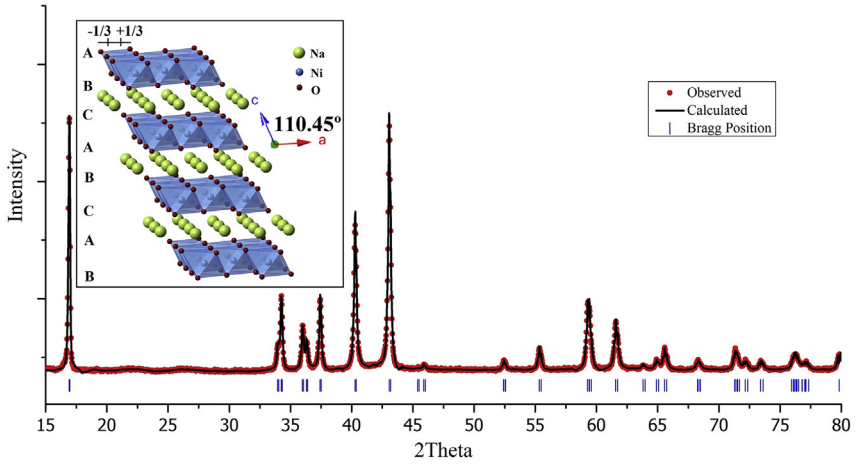

Fig. 1. XRD pattern matching of pristine $NaNiO_2$ powder: experimental pattern (dotted curve), refined profile (continuous line), and Bragg positions (vertical bars). The crystal structure of O′3 monoclinic is shown in inset, and the radii of each element are not in scale.

pattern in a 2θ range of 15–80°. The cells were relaxed for 30 min before each XRD measurement.

3. Results and discussions

The layered structure of pristine monoclinic O′3-phase $NaNiO_2$ is shown in the inset of Fig. 1. Octahedrally coordinated Na ions are located in between the NiO_6 layers where the oxygen stacking follows an ABCABC sequence to form 3 octahedral environments for sodium ions. Na–O_6 octahedra share one edge and one face with upper and lower NiO_6 octahedra [6]. At room temperature, the O′3-phase may undergo a series of phase transitions during the electrochemical deintercalation/intercalation reaction because each layer can glide along the *a*- and *b*-axis to form more stable phases at a certain charge/discharge voltage with a certain sodium concentration range. These transformations will be reflected as step behaviours in the charge/discharge curve and could imply structural instability at extensive cycling. The obtained XRD pattern of pristine monoclinic $NaNiO_2$ shown in Fig. 1 is fitted with FullProf software using *C*2/*m* symmetry, and the cell parameters are calculated to be $a = 5.323(4)$ Å, $b = 2.845(2)$ Å, $c = 5.583(5)$ Å, and $\beta = 110.44(4)°$, which are in excellent agreement with previously published literature values ($a = 5.33$ Å, $b = 2.860$ Å, $c = 5.59$ Å, and $\beta = 110.5°$) [8]. The *a* and *c* parameters represent the diagonal and the edge distance of an MO_6 octahedron respectively [3]. Since the transition metals are octahedrally coordinated by oxygen to form a hexagonal lattice, the lattice parameters are expressed with *a* (monoclinic) = $\sqrt{3}a$ (hexagonal) and *b* (monoclinic) = *a* (hexagonal) [12]. Therefore, the *a*/*b* ratio of an ideal hexagonal system is $\sqrt{3}$ (1.73) and any deviation from this ratio is an indication of distortion [12]. The *a*/*b* ratio of pristine $NaNiO_2$ (1.88), along with the β angle (110.45°) clearly indicates a remarkably strong Jahn–Teller distortion induced by Ni^{3+} in low spin configuration ($t_{2g}^6\ e_g^1$). This highly distorted monoclinic phase is stable at room temperature while the ideal rhombohedral phase becomes stable at or above 450 K because thermal energy can overcome the Jahn–Teller defect at high temperature [10].

When the slurry of the electrode is prepared with a mixture of NMP and PVDF, a partially desodiated phase forms even before any electrochemical cycling, which is indicated by the appearance of a second (001) reflection at a lower angle as shown in Fig. 2 inset a. This phase has been previously identified as $Na_{0.91}NiO_2$ [10]. The formation of a partially desodiated phase upon preparation of the electrode is probably due to the highly hygroscopic nature of pristine $NaNiO_2$. Since NMP is completely miscible with water, even a small amount of moisture contamination could contribute to the formation of this partially desodiated phase during slurry preparation. Indeed, when the electrode slurry is prepared with a mixture of EPDM and cyclohexane in an Ar-filled glove box, the formation of this partially desodiated phase is vastly suppressed as shown in Fig. 2 inset b, which suggests the necessity of a completely dry environment when handling the pristine material. Furthermore, when an extensive amount of sodium is deintercalated from the crystal, the electrodes exhibit an extra peak at 25.6° which is known as the highly swollen peak [13], due to penetration of H_2O into the interlayer even though the electrodes are protected by Kapton film during the *ex situ* XRD measurement (see Supporting information S-1). Therefore the study of the structural evolution of $NaNiO_2$ upon electrochemical cycling has been carried out using an *in situ* cell.

Fig. 3 is a typical 1st charge/discharge curve of $NaNiO_2$ within the voltage range of 4.0–1.5 V at C/10. With OCV (open circuit voltage) at 2.56 V, the 1st charge capacity reached 160 mA h g^{-1} and the following discharge capacity reached 114.6 mA h g^{-1}, values that are comparable to those reported in a recent publication [10] considering the narrower electrochemistry window in the current study. The polarization during the charge/discharge process is approximately 100–300 mV. During the 1st charge 4 bold plateaus are observed, implying multiple phase transitions due to the gliding of oxide layers, changes in degree of distortion when sodium is deintercalated from the structure or rearrangement of sodium ions in the interlayer space during the charge/discharge cycle as shown in the $NaVO_2$ system [14]. These plateaus, marked a to d, correspond to OCVs of 2.59, 3.04, 3.38, and 3.53 V respectively. During the discharge, 4 bold plateaus are also observed that are similar in step behaviour to that of the plateaus observed in the charge process. The shape of each plateau during the discharge process is almost identical to that of the charge process, indicating that the phase change during the electrochemical process is highly reversible. It should be noted however that the 1st discharge capacity is significantly lower than that of 1st charge capacity. It is well documented that during the 1st discharge process, the fully sodiated phase cannot be achieved [10], and therefore, a significant loss of capacity is observed. Indeed, the length of each plateau, marked a to d and a′ to d′ to in Fig. 3, is approximately the same during the charge and discharge process except for the 1st plateau (a for charge and a′ for

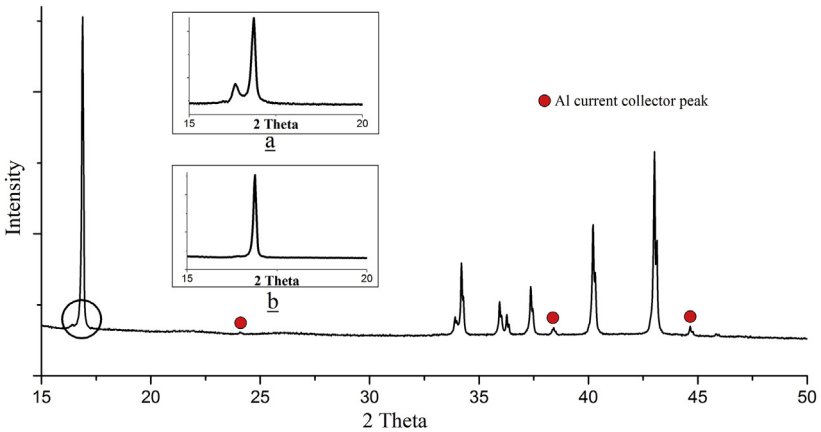

Fig. 2. XRD pattern of a laminate electrode prepared with EPDM in cyclohexane. Insets are amplified views ($2\theta = 15°–20°$) of a) the laminate prepared with PVDF in NMP and b) the laminate prepared with EPDM in cyclohexane.

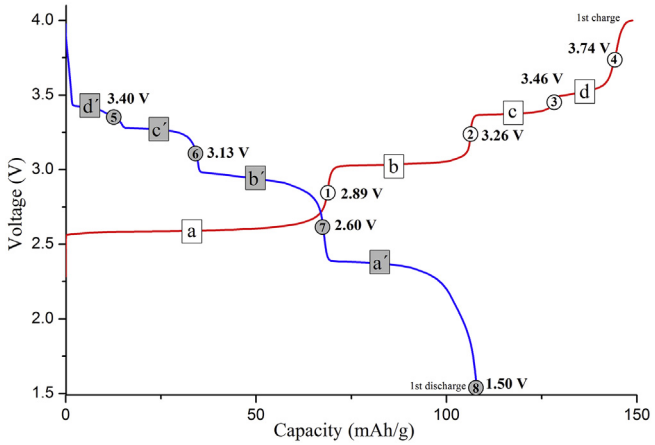

Fig. 3. Typical first charge/discharge cycle of $NaNiO_2$ within the voltage range of 4.0–1.5 V at C/10 rate. Numbers ① to ⑧ indicate the voltage stop at which *ex situ* and relaxed *in situ* XRD experiments are performed and a to d´ indicates corresponding plateaus during charge/discharge process.

discharge). A deep drop occurs below 2.3 V which implies that it requires a significantly unfavourable phase transition in order to achieve the fully sodiated phase.

Real-time *in situ* XRD measurements of powder electrode have been performed within the 2θ range of 15–18° and 31–38° as seen in Fig. 4. The first scan clearly indicates that the pristine material is pure $NaNiO_2$. However, as soon as the charge process starts, the fully sodiated phase starts disappearing rapidly and partially desodiated phases start dominating, indicated by the shift of (001) reflection toward lower 2θ angle. Ranging from approximately 1.0 to 0.74 sodium ions per formula unit, O′3, P′3 and O‴3-phases are observed. The latter, not reported previously, appears briefly at the beginning of charge and subsequently transforms into P′3 structure (see Supporting information S-2). This new phase is more noticeable at the end of the discharge process. In order to complement the real-time *in situ* XRD data, the relaxed *in situ* XRD pattern has been collected at 2θ range of 15–80° while stopping the cell at each voltage indicated by numbers ① to ⑧ in Fig. 3. While real-time *in situ* XRD provides visual evidence of on-going phase transition, more detailed information regarding the crystal structure at each transition is obtained with relaxed *in situ* experiments at the selected voltages because a wider range scan is performed (see Supporting information S-2). The shift of (001) reflection toward lower angle indicates that the c-spacing increases as sodium is being deintercalated from the host material because deintercalation of sodium increases repulsion between each oxide layers due to removal of positively charged sodium ions [5]. In addition, the shift of (−201) reflection towards smaller *d*-spacing indicates that the *a* shrinks due to increasing concentration of the smaller Ni^{4+} ion, as does the *b*-axis. In order to establish the structural type of the new phase, both O3 and P3 structures have been used to fit the XRD patterns and the distorted O3 phase gives the best fitting based on relaxed XRD data. It has a β angle of 111.3° and an a/b ratio of 1.71, which are values in between those of O′3- and P′3-phases. However, the *b* parameter and consequently the volume are slightly bigger compared to the other P- or O-phases. Since the new phase differs in cell parameters from the other monoclinic O3 phases previously reported is designated as O‴′3.

Moving forward, a new biphasic region appears in the sodium concentration range between $x = 0.74$ and 0.55, where P′3 and P″3 phases coexist. The relaxed *in situ* XRD measurement indicates that at 3.26 V (see Supporting information S-2), which corresponds to 0.55 sodium concentration, almost all O′3- and P′3-phases have disappeared and the new P″3-phase has become the major component (see Supporting information S-3 and S-4). Indicated by double prime, this transition is the result of increasing degree of distortion, where the a/b ratio increases from 1.73 to 1.76. However, the β angle does not change much ($\beta = 121.5°$) because the crystal system still prefers a hexagonal crystal system. Further oxidation leads to a new plateau at 3.38 V within the sodium concentration range 0.55–0.42 in which the coexistence of three phases, P″3, P‴3, and O″3, has been found. Indeed, P″3 transforms into a new distorted P3 phase before O″3 forms, as shown in Fig. 4. This new phase, which has only been observed during the charge redox reaction, is designated as P‴3 as it is slightly more distorted than the P″3-phase, yet does not result

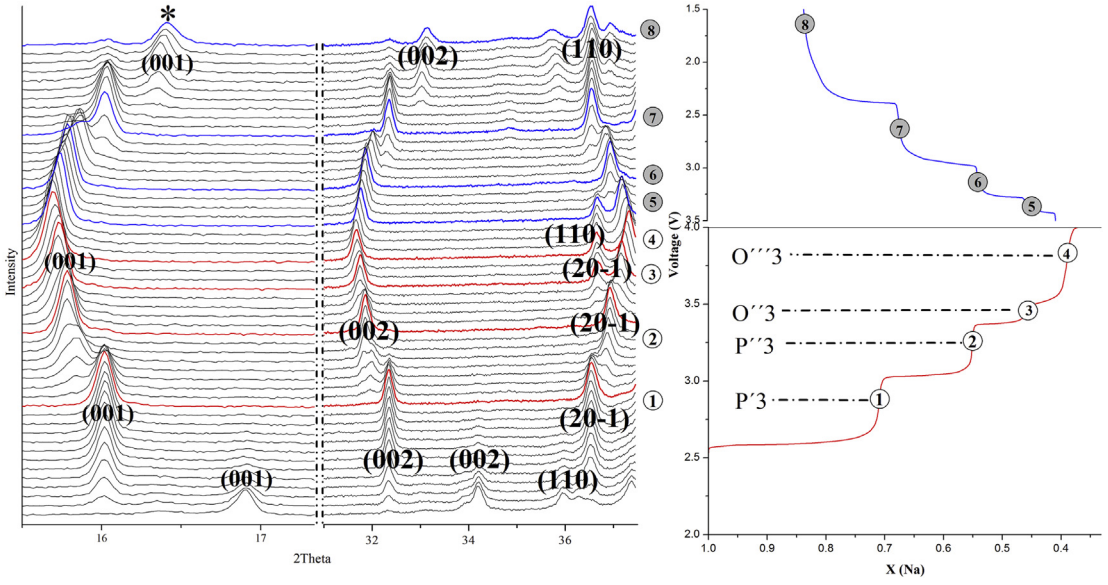

Fig. 4. *In situ* XRD patterns of electrode during the 1st charge/discharge process and voltage composition curve with corresponding phase transitions.

in a good fit using the O″3 structural model. The a/b ratio from P‴3 to O″3 does not change much but the β angle changes dramatically from 119.75° to 106.0° because this transition involves changing from a hexagonal to a monoclinic crystal system. Deintercalating extensive amount of sodium from the interlayer is known to dramatically increase repulsion between adjacent layers that are facing each other and induces a P- to O-phase transition as seen in P2 to O2 transitions in P2-phase $Na_xNi_{1/3}Mn_{2/3}O_2$ [15]. There is a small biphasic region of O″3 and O‴3 within 0.42–0.40 sodium concentration but it quickly changes to a solid solution of O‴3. As seen in the relaxed *in situ* XRD scan at the voltage of 3.74 V, O′3, P′3, P″3, and O″3 peaks have almost completely disappeared and only the O‴3-phase can be observed down to approximately 0.37 sodium. Note that the transition from O″3 to O‴3 is the only region where the c-spacing slightly decreases (see Table 1) while more sodium is removed, as has been already reported in previous literature [9].

The subsequent discharge profile exhibits a similar behaviour to that of the charge process, including the phase transitions and the voltage values at which the transitions occur. However, the polarization becomes larger as the discharge voltage approaches 2.3 V, indicating that the electrochemical intercalation of sodium into the host structure becomes kinetically unfavoured as sodium concentration approaches its pristine state. This large polarization along with the dramatic voltage drop below 2.3 V implies that obtaining the fully sodiated phase via electrochemical reaction is highly unlikely [10]. As in the charge process, at 2.3 V and below, the new O⁗3 phase becomes visible, marked as * in Fig. 4, which proves that it is possible to go beyond P′3-phase upon discharge, contrary to what was previously believed [10]. More detailed studies as to the limit of sodium insertion and its kinetics as well as isolating the new phase by chemical oxidation for a more complete structural characterization are under way. The summary of the phase transitions, cell parameters, and sodium contents obtained from XRD and electrochemical experiments are included in Table 1. All the cell parameters are in excellent agreement with previously reported results [9], but significantly different sodium contents in each phase have been found. The previous report showed electrochemically reversible deintercalation/intercalation reaction from 1.0 to 0.8 sodium ions while the current study shows deintercalation up to $Na_{0.37}NiO_2$ at 4.0 V. A recent publication shows that even more sodium ions could be deintercalated at 4.5 V although the electrochemical reaction became highly irreversible [10]. ICP measurements of electrodes at selected state of charge/discharge show good agreements with the corresponding sodium contents based on electrochemistry (see Supporting information S-5). The revision of sodium contents in each phase transition is thus also included in Table 1. The cell parameter evolution of each phase as a function of sodium concentration based on real-time *in situ* XRD analysis is represented in Fig. 5.

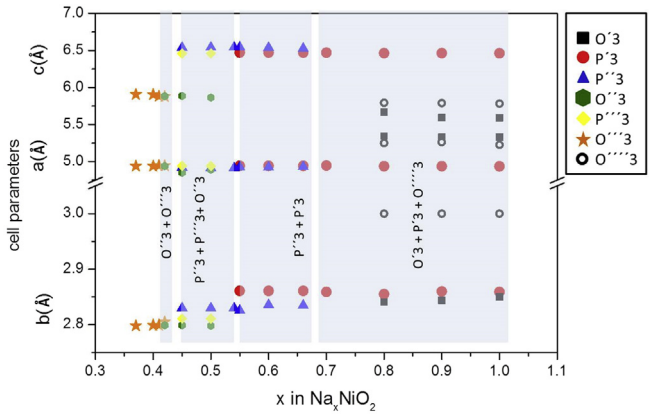

Fig. 5. *In situ* evolution of the refined cell parameters of the different phases encountered during the first charge of the real-time *in situ* experiment plotted as a function of Na content. Shadowed areas indicate two-phase and three-phase regions.

Fig. 6a) is a plot of voltage as a function of capacity during the first 3 cycles within the voltage range of 4.0–2.0 V at C/10 rate. A considerable first cycle irreversibility is observed due to the difficulty to form the O′3 structure upon Na^+ intercalation, as already mentioned. After the first cycle the capacity loss is moderate with retention of approximately 89% for charge/discharge process from 2nd to 25th cycle along with a constant coulombic efficiency of 98% up to 25 cycles (see Fig. 6b)). Such a good coulombic efficiency discards electrolyte decomposition as the source of capacity decay, which could be rooted in the structural transitions instead although further work is ongoing to clarify these aspects.

4. Conclusions

We report the successful synthesis of monoclinic $NaNiO_2$ and *ex situ*, real-time and relaxed *in situ* XRD analysis of the phase transitions during the 1st charge/discharge cycle. The 1st charge capacity reaches 160 mA h g^{-1} while 114.6 mA h g^{-1} is obtained in the following discharge within the voltage range of 4.0–1.5 V at C/10. During the charge and discharge process, multiple phase transitions O′3-P′3-P″3-O″3-O‴3 are observed. The cell parameters corresponding to each different phase are found to be in excellent agreement with the previous report. However, the sodium contents in each phase are herein revised because desodiation up to $Na_{0.37}NiO_2$ is achieved in the current study as opposed to only $Na_{0.8}NiO_2$ in the previous report [9] within a similar voltage range. In addition, two new phases, designated as P⁗3 and O⁗3, have been discovered at high voltage during the charge and at low voltage during the charge and discharge processes respectively. It has been widely believed that during the discharge, a phase beyond P′3-phase cannot be observed.

Table 1
Sodium content, phase and cell parameters comparison between Braconnier's [9] and current study.

Phase	Na content		Cell parameters						Volume (Å^3)	Voltage (V)
	Braconnier	Current study	a (Å)	b (Å)	c (Å)	β (°)	a/b	c-Spacing (Å)		
O′3	$Na_{1.00}NiO_2$	$Na_{1.00}NiO_2$	5.3282(6)	2.8484(2)	5.5833(8)	110.43(2)	1.87	5.23	79.02	2.25
O⁗3	N/A	$Na_{0.83}NiO_2$	5.2254(7)	3.0462(7)	5.7831(2)	111.264(5)	1.71	5.39	85.90	2.25
P′3	$Na_{0.91}NiO_2$	$Na_{0.70}NiO_2$	4.945(4)	2.865(1)	6.466(2)	121.62(3)	1.73	5.51	77.85	2.89
P″3	$Na_{0.84}NiO_2$	$Na_{0.55}NiO_2$	4.934(2)	2.802(2)	6.569(6)	121.46(8)	1.76	5.60	77.21	3.26
P⁗3	N/A	$Na_{0.50}NiO_2$	4.94(9)	2.81(2)	6.46(5)	119.8(2)	1.76	5.61	77.81	3.38
O″3	$Na_{0.81}NiO_2$	$Na_{0.45}NiO_2$	4.9054(5)	2.794(3)	5.863(3)	106.912(5)	1.75	5.61	76.92	3.46
O‴3	$Na_{0.79}NiO_2$	$Na_{0.37}NiO_2$	4.933(1)	2.7948(5)	5.890(7)	107.52(2)	1.76	5.62	77.67	3.74

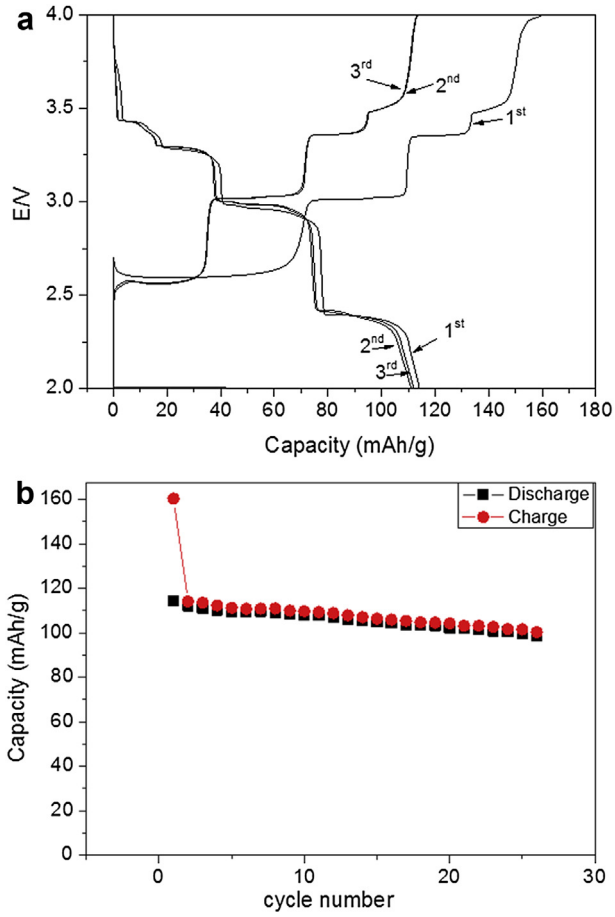

Fig. 6. a) Voltage vs. capacity of a Na/$NaNiO_2$ at C/10 rate. b) Cycling stability and the capacity obtained for $NaNiO_2$ at C/10 rate after 25 cycles.

However, the discovery of the O′′′′3 phase implies the possibility of obtaining a phase closer to the fully sodiated phase during the electrochemical cycle. The capacity remained 89% with coulombic efficiency of 98% from 2nd to 25th cycle within the voltage range of 4.0–2.0 V at C/10 which indicates the feasibility of $NaNiO_2$as a Na-ion battery cathode material.

Conflict of interest

The authors declare no competing financial interest.

Acknowledgements

Dr. Damien Saurel and Mr. Egoitz Martin are acknowledged for meaningful discussions about the XRD refinements and assistance with the *in situ* XRD experiments. In addition, we thank Ms. Guen Hwa Han for proofreading our manuscript. This work was supported by the Basque Government through the Etortek project energigune'10 grant.

Appendix A. Supplementary data

XRD analysis data and ICP results on selected compositions are available. Supplementary data associated with this article can be found in the online version, at http://dx.doi.org/10.1016/j.jpowsour.2014.02.048.

References

[1] V. Palomares, P. Serras, I. Villaluenga, K.B. Hueso, J. Carretero-Gonzalez, T. Rojo, Energy Environ. Sci. 5 (2012) 5884.
[2] V. Palomares, M. Casas-Cabanas, E. Castillo-Martínez, M.H. Han, T. Rojo, Energy Environ. Sci. 6 (2013) 2312.
[3] A. Mendiboure, C. Delmas, P. Hagenmuller, J. Solid State Chem. 57 (1985) 323.
[4] C. Delmas, J.-J. Braconnier, C. Fouassier, P. Hagenmuller, Solid State Ionics 3/4 (1981) 165.
[5] Y. Takeda, K. Nakahara, M. Nishijima, N. Imanishi, O. Yamamoto, Mater. Res. Bull. 6 (1994) 659.
[6] C. Delmas, C. Fouassier, P. Hagenmuller, Physica B 99 (1980) 81.
[7] P. Kalyani, N. Kalaiselvi, Sci. Technol. Adv. Mater. 6 (2005) 689.
[8] M.S. Whittingham, Chem. Rev. 104 (2004) 4271.
[9] J.J. Braconnier, C. Delmas, P. Hagenmuller, Mater. Res. Bull. 17 (1982) 993.
[10] P. Vassilaras, X. Ma, X. Li, G. Ceder, J. Electrochem. Soc. 160 (2013) A207.
[11] J. Rodríquez-Carvajal, Physica B 192 (1993) 55.
[12] S. Miyazaki, S. Kikkawa, M. Koizumi, Synth. Met. 6 (1983) 211.
[13] X. Yang, K. Takada, M. Itose, Y. Ebina, R. Ma, K. Fukuda, T. Sasaki, Chem. Mater. 20 (2008) 479.
[14] C. Didier, M. Guignard, C. Denage, O. Szajwaj, S. Ito, I. Saadoune, J. Darriet, C. Delmas, Electrochem. Solid-State Lett. 14 (2011) A75.
[15] D.H. Lee, J. Xu, Y.S. Meng, Phys. Chem. Chem. Phys. 15 (2013) 3304.